SPECTRAL ANALYSIS OF ASTER, HYPERION, AND QUICKBIRD DATA FOR GEOMORPHOLOGICAL AND GEOLOGICAL RESEARCH IN EGYPT (DAKHLA OASIS, WESTERN DESERT)

G. Waldhoff [a, *], O. Bubenzer [b], A. Bolten [a], W. Koppe [c], G. Bareth [a]

[a] Dept. of Geography, University of Cologne, Albertus-Magnus-Platz, 50923 Cologne, Germany - (guido.waldhoff, andreas.bolten, g.bareth)@uni-koeln.de
[b] Dept. of Geography, University of Heidelberg, Im Neuenheimer Feld 348, 69120 Heidelberg, Germany - olaf.bubenzer@geog.uni-heidelberg.de
[c] Infoterra GmbH, 88039 Friedrichshafen, Germany - wolfgang.koppe@infoterra-global.com

Commission VIII, WG VIII/12

ABSTRACT:

This paper presents an evaluation, to which degree geological and geomorphological information can be obtained from modern remote sensing systems like the multispectral ASTER or the hyperspectral Hyperion sensor for a hyperarid desert region like the Dakhla Oasis (Western Desert, Egypt). To account for the enhanced information content these sensors provide, hyperspectral analysis methods, incorporating for example Minimum Noise Fraction-Transformation (MNF) for data quality assessment and noise reduction as well as Spectral Angle Mapper (SAM) for classification, were applied. As compensation for ground truth data high spatial resolution Quickbird data was obtained, too. The classification results show that detailed information can be extracted from the data, which were compared with the Geological Map of Egypt 1:500.000. Regarding the data quality, the analysis revealed that the Hyperion scene was strongly affected by system induced radiometric interferences. As a result, a considerable amount of bands had to be discarded to allow satisfying results. Therefore, although similar surface types were discriminated with the ASTER and the Hyperion results, the ASTER data allowed a more detailed classification of the surface composition of the study area. Additionally, ASTER elevation data was used to relate the classification results with the relief of the study area.

1. INTRODUCTION

Detailed information on surface morphology or information about bedrock properties of remote arid regions are important issues for many topics investigated in interdisciplinary research projects like 'Arid Climate, Adaptation and Cultural Innovation in Africa' (ACACIA, http://www.uni-koeln.de/sfb389). This counts in particular for regions like the Dakhla Oasis (Western Desert, Egypt), where geological or geomorphological information is only available for small areas, where field data were collected. For larger areas, such information is (if any) only available in an unsatisfactory resolution. Hence, modern satellite borne remote sensors as the multispectral 'Advanced Spaceborne Thermal Emission and Reflection Radiometer' (ASTER) and the hyperspectral Hyperion can provide an important contribution in gaining such information. To evaluate, which information can be extracted from these datasets for a regional scale, the remote sensing analysis results will be compared with the Geological Map of Egypt 1:500.000 sheet NG 35 SE Dakhla' (Klitzsch, et al. 1987), which is the best source of spatial geological and also gemorphological information for the study area until today. While ASTER and Hyperion allow the spectral analysis for the mapping of surface types, high spatial resolution Quickbird data is used for visual image interpretation of experts with field knowledge, as a compensation for ground truth data. By comparing the specifications of ASTER and Hyperion, it is expected that

Hyperion (as being a hyperspectral sensor with multiple bands) should enable superior mapping results, while ASTER provides stereo image data to generate digital elevation models (DEM) enabling geomorphological analysis.

2. GEOMORPHOLOGICAL & GEOLOGICAL SETTING OF THE STUDY AREA

The Dakhla Oasis is located in the Western Desert of Egypt (Fig. 1). The climate in this part of the eastern Sahara is hyperarid with an average annual rainfall of below 1 mm (EMA 1996). Thus, the region is almost devoid of vegetation outside of the Oases. The study area is situated along the settlements Balat and Teneida in the eastern part of the Oasis. According to Brookes (1993), the study area can be divided into four major geomorphological sub-regions from north to south: (i) in the north, the tertiary Egyptian Limestone Plateau arises up to 550 m above sea level (asl) (derived from SRTM data, CGIAR 2004) consisting mainly of palaeocene formations. On the plateau a major aeolian relief is developed, mainly consisting of broad meter-deep channels and of up to tens of meters high yardangs running in NNW-direction (Brookes 2001). (ii) to the south, the plateau is bordered by a distinct escarpment, which mainly strikes east to west. The upper face of the scarp (about 20-40 m thick) is build by the limestone formations, while the lower segment is composed of

---

* Corresponding author.

thick layers of the cretaceous Dakhla shales. (iii) the scarp surface is carved by deep wadis, which descend through a piedmont zone towards the Dakhla Lowland below 140 m asl were the settlements are situated. (iv) further south, the lowland is confined by a low cuesta, followed by a wide plain, whose underground is composed of the older cretaceous Nubian Sandstone, while the surface is covered by sand sheets.
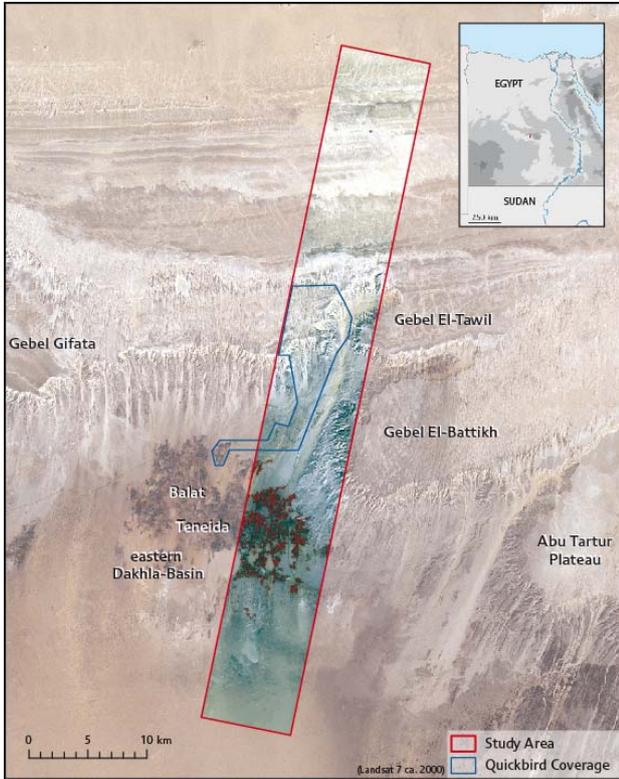
Figure 1. Location of the Study area (ASTER 2006)

Likewise, many other parts of the study area are covered by quaternary deposits such as aeolian sand or colluviums in the range of the scarp and the piedmont zone.

3. REMOTE SENSING DATA & PREPROCESSING

The multispectral 'Advanced Spaceborne Thermal Emission and Reflection Radiometer' (ASTER) onboard the TERRA satellite has three bands in the VNIR (15 m) and six bands in the SWIR (30 m) wavelength region (Fig. 2) (Fujisada 1995). In particular, the SWIR bands were intended for the discrimination of minerals or rock types (Yamaguchi et al. 1998). Additionally, ASTER provides along-track digital stereo image data at 15 m resolution to produce relative digital elevation models with 30 m spatial resolution (Fujisada et al. 2001, 2005). With an elevation error of only approx. 6 m, they are suitable for scales up to 1:50.000 (Bolten and Bubenzer 2006, Hirano et al. 2003). Thus, high resolution elevation data of the study area could be used. For the spectral analysis, a L1B-ASTER scene ('Registered Radiance at the Sensor') from February 20, 2006 was acquired (Abrams 2000, Ersdac 2003a). The preprocessing of the ASTER data comprised the radiometric correction for sensor crosstalk of the SWIR-Instrument (Iwasaki et al. 2002), the combination of the VNIR and SWIR instrument data to a 9-band-imagecube, and the

atmospheric correction to assure a better comparability to the Hyperion data. The correction of the SWIR-bands with the Crosstalk Correction Software provided by Ersdac (2003b, Iwasaki and Tonooka 2005) is particularly important, due to the significant absorption features, which minerals or rock types exhibit in the SWIR region (Clark 1999). The four ASTER bands in the thermal infrared (TIR) were not utilized in this study. For the production of the ASTER DEM, with PCI Geomatica Orthoengine 9, the raw L1A-data of the ASTER scene was used. This data product comes along with the stereo bands 3N & 3B plus geometric ancillary parameters required for the DEM generation (Fujisada et al. 2001).
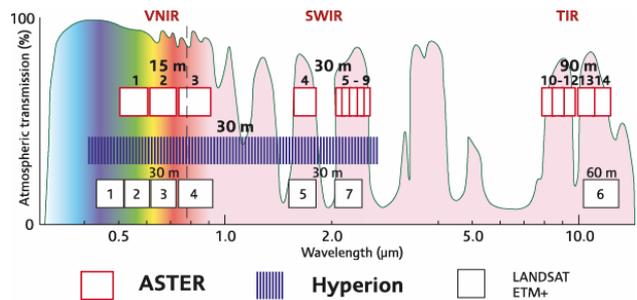
Figure 2. ASTER and Hyperion spectral bands compared to Landsat ETM+ (after Kääb et al. 2002, modified)

The Hyperion sensor, onboard NASA's EO-1 platform, is the first spaceborne imaging spectrometer covering the wavelength region from 0.4 to 2.5 µm (as depicted in Fig. 2) with 220 bands of 10 nm spectral resolution and 30 m spatial resolution (Folkman et al. 2001, Ungar et al. 2003). In this way, hyperspectral data is available at comparatively low costs especially for remote areas. For the current study, L1R-Data ('at-sensor radiance') of March 16, 2003 was acquired. Due to signal-to-noise issues and other radiometric detractions only 198 bands are calibrated in this data product (for further details see Pearlman et al. 2003). In addition, the data comes with a flag mask assigning bands with limited radiometric quality. The visual inspection of the single Hyperion bands during the preprocessing revealed further serious radiometric errors like severe stripping in some SWIR bands (typical for pushbroom sensors, Fig. 3) as well as the spectral smile (a shift of the sensitivity of some detectors in cross-track direction), affecting mainly the bands in the VNIR region.
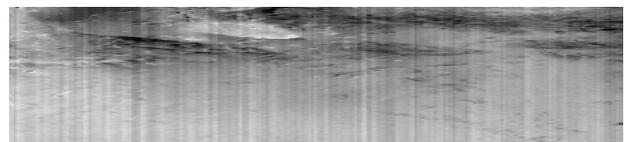
Figure 3. Hyperion band 63 (SWIR) affected by Striping

A detailed description of the radiometric errors observed in Hyperion data is presented by Datt et al. 2003 or Binschadler and Choi 2003. Unfortunately, a software that might have helped correcting the radiometric errors (Khurshid et al. 2006) was not available for this study. As a result, only a subset of 158 bands, still containing bands with radiometric interferences, was maintained for further analysis. An atmospheric correction was applied to the Hyperion scene as well.

In contrast to the other sensors, Quickbird operates four multispectral bands plus a pan channel, covering the VNIR portion of the electromagnetic spectrum with a spatial resolution of 0.61 cm for pan-sharpened products, which was the highest resolution of a spaceborne sensor available during the investigation (Digitalglobe 2006). Consequently, Quickbird provides image data approximating the quality of aerial photography and enabling visual image interpretation. For the study, pan-sharpened 'Standard Imagery' of February 23, 2004 was used. This data product is already radiometrically and geometrically corrected, so no further preprocessing was carried out. Due to the high data costs, the Quickbird coverage could only be obtained for selected areas (Fig. 1).

After completing the preprocessing of all datasets, a coregistration and subsetting of the scenes to the extent of the study area was applied.

4. METHODS

Due to the increased number of bands hyperspectral sensors like Hyperion or even modern multispectral sensors like ASTER provide, new analysis methods have become available in recent years (Broadman 1993, Kruse et al. 2003, Chang 2003, Van Der Meer et al. 2003). To account for the improved information content of the new generation sensors, hyperspectral analysis techniques were chosen for the study for both datasets. These methods are based on the fact that every material exhibits a unique spectral signature in the electromagnetic spectrum. If sufficient bands are available in the remote sensing data, these signatures can be reconstructed. Thus, for mapping the surface composition, image derived reflectance spectra of the pictured earth surface are compared to (known) reference spectra of materials, also referred to as endmembers (Adams and Gillespie 2006). Endmembers can be obtained from different sources like field measurements, spectral libraries (e.g. ASTER spectral library: http://speclib.jpl.nasa.gov) or from the image data itself. In the latter case, surface type identification can be achieved e.g. by comparing the image spectra with spectra of known areas or with library spectra.

To evaluate the selected methodology and the classification results that can be achieved with ASTER and Hyperion data, two different methods for the selection of endmembers were applied in this study (Fig. 4). The first method is mainly based on the 'Spectral Hourglass' processing scheme (Kruse et al. 2003) which is implemented in the Software ENVI (Research Systems Inc. 2005). This Procedure includes the generation of Minimum Noise Fraction-Images (MNF) for data dimensionality estimation and reduction by decorrelating the useful information and separating noise (Green et al. 1988), Pixel Purity Index-Mapping (PPI) for the determination of the purest pixels in an image (as potential endmembers) utilizing the (uncorrelated) MNF-images and finally the extraction of endmembers (referred to as n-D-endmembers in the following) utilizing the n-Dimensional-Visualizer tool (n-D-Vis). The extracted endmembers were then compared to known spectra from spectral libraries for identification. Subsequently, an alternative endmember selection was performed by the visual interpretation of the Quickbird data. In this case, locations regarded as representative for a surface type, were marked as Regions-of-Interest (ROI) in the Quickbird image. These ROIs were then transferred to the ASTER and Hyperion datasets to serve as sources for the extraction of endmembers as well

(ROI-endmembers). In this approach, the endmembers for both datasets were derived from the same spatial source.
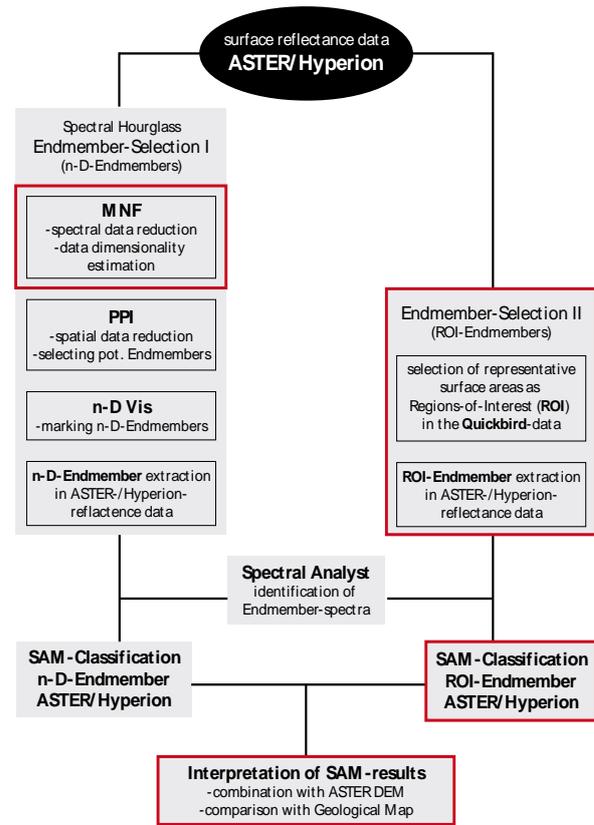
Figure 4. Analysis methodology of the study (presented analysis steps in red)

For the mapping of the surface composition the Spectral Angle Mapper (SAM) was chosen. SAM is a physically-based classification algorithm that compares the spectral similarity between (surface) reflectance image spectra and reference spectra, treating them as vectors in a space with the dimensionality equal to the number of bands (Jensen 2005). Image spectra are assigned to the reference spectrum class that yields the smallest calculated angle. One advantage of the algorithm is that it is insensitive to relative brightness differences of pixels belonging to the same feature type (Kruse et al. 1993, Research Systems Inc. 2005). Finally, the classification results were combined with the ASTER DEM, in order to relate certain surface types to the relief.

5. RESULTS & DISSCUSSION

5.1 Spectral Hourglass processing scheme

Results showed that the endmembers derived with the Spectral Hourglass methodology were not able to reveal the information content of both (ASTER & Hyperion) datasets (Waldhoff 2006). Therefore, this paper concentrates on the analysis results using the roi-endmembers. Nevertheless, the generation (and inspection) of MNF-images, as the first step in the Spectral Hourglass procedure, was very helpful for the evaluation of the inherent information content (data dimensionality) of both remote sensing datasets. Usually the first few MNF bands convey the most information, while subsequent bands

increasingly contain noise. MNF bands with calculated eigenvalues below one usually do not carry useful information and contain mainly noise (Jensen 2005). In the case of ASTER, a data dimensionality of above one was calculated for all bands. Thus, no bands were excluded. Regarding the Hyperion data, the MNF-Transformation, and the subsequent visual inspection revealed again that much more bands were affected by the radiometric distortions. Therefore, in order to enable satisfying results, MNF bands carrying strong radiometric disturbances had to be excluded from the analysis, although some of these bands had relatively high eigenvalues and probably also contained valuable information. As a result, only a subset of six selected MNF-bands was maintained. This subset of MNF bands was then retransformed to reflectance data (inverse MNF) for the classification (Green et al. 1988, Research Systems Inc. 2005). The resulting reflectance dataset contained 158 bands again, but only with the spectral information of the chosen MNF bands.

5.2 ROI-Endmember selection

For the classifications, 12 endmembers of surface types that could be recognised in the Quickbird image were transferred to the ASTER and Hyperion datasets (Fig. 5). The ROIs were
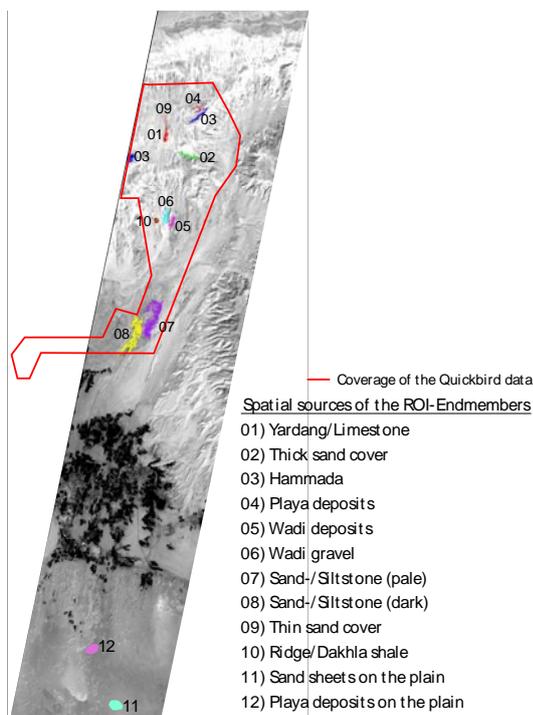
Figure 5. ROIs selected in the Quickbird image for the extraction of endmembers

chosen on the assumption, that a structural relief is predominant in the reserach area and therefore distinct geomorphological features (e.g. the class Yardang) are connected to the petrography of the region (Olaf Bubenzer 2006, personal communication). Since, several surfaces identified as sand cover, appeared visually and spectrally different in the data depending on their location or possibly even their thickness, more than one endmember had to be taken for the surface type sand cover. Additionally, the visual inspection of the MNF bands revealed, that a heterogeneous surface composition could also be expected in the southern part,

outside the Quickbird coverage. Therefore, ROIs lying outside of the coverage were added.

5.3 Classification results and interpretation

Fig. 6 and Fig. 7 depict the classification results using the roi-endmembers for the ASTER and the Hyperion data, respectively. The comparison of the classification results show that most surfaces were similarly differentiated, although some parts are assigned to different classes.
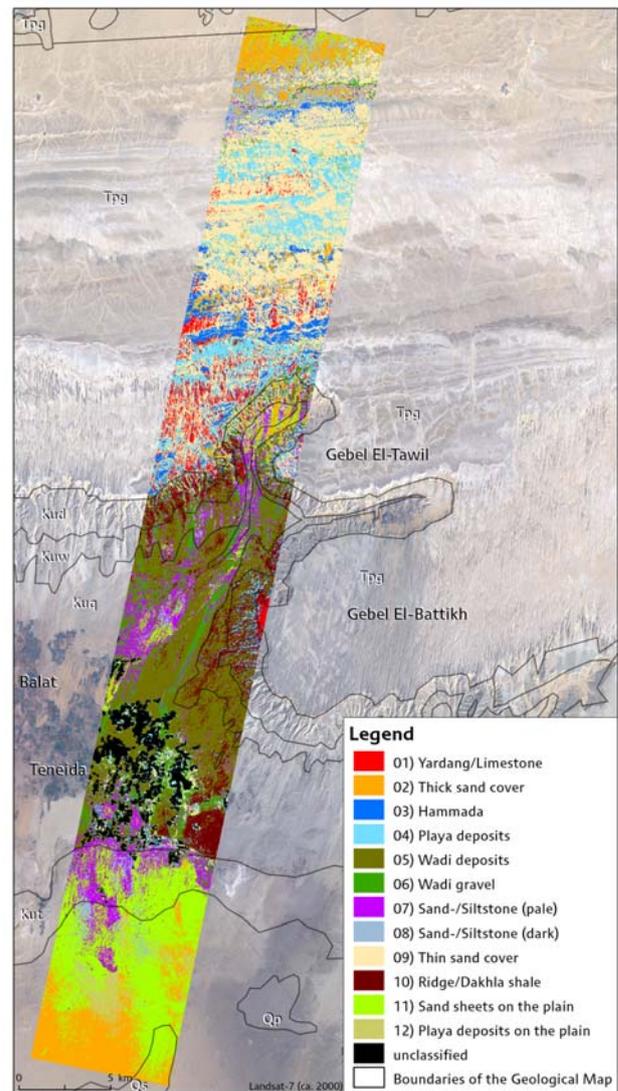
Figure 6. SAM-Classification result of the ASTER data

Regarding Hyperion, the classification was affected by the radiometric errors, as well. For example, residuals of the striping are visible in some parts, while the differentiation of classes seemed to be "blurred" in other regions in comparison to the ASTER classification. On the other hand, the ASTER result displays a more detailed picture in general. In both classifications, noticeably many parts of the study area are assigned to classes that represent different types of quaternary deposits, in particular aeolian sand. This indicates, that much bigger regions are covered by quaternary sands, than assigned

in the geological map, which sometimes hampers inferences regarding the geology.

However, while the study area can be structured generally into similar regions in comparison to the geological map, in particularly for the Limestone Plateau in the northern half of the study area, much new information could be extracted from the classifications (see polygon boundaries in Fig. 6 & Fig. 7).
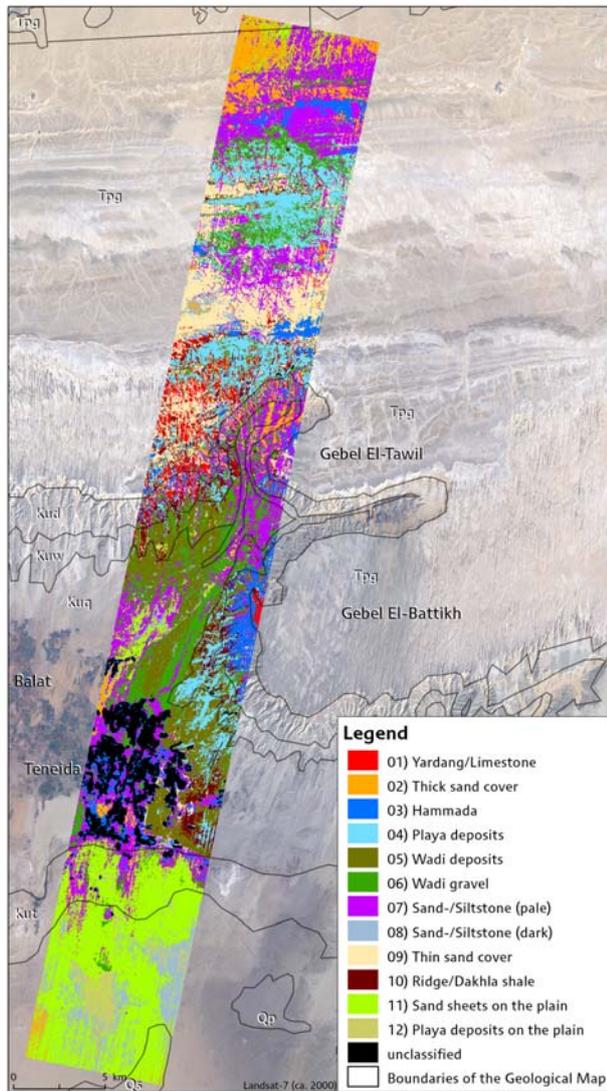
Figure 7. SAM-Classification result of the Hyperion data

While the geological map delineates only one formation for this region, both classifications results display a much more heterogeneous surface composition, consisting mainly of the surface types Yardang (01), sand filled troughs (09 Thin sand cover) and desert pavement (03 Hammada). In this regard, especially the mapping of the Yardang class worked particularly well. But also the differentiation of the major geomorphological sub-regions as described by Brookes (1993) were reflected by the classification. Additionally, through the connection of the classifications with the ASTER DEM, the existence of several small scarps on the plateau (Brookes 1993) could also be derived from the data (Waldhoff 2006).

6. CONCLUSION

It was of central importance for the study, which geological and geomorphological information can be extracted from the modern remote sensing datasets for arid regions. In this regard, new detailed information were extracted from the classifications to update the geological map. The appearances of both classification results indicate that even for unknown arid regions, multiple information can be gained from modern sensors like ASTER and Hyperion. Regarding the data quality, the Hyperion result suffered from the partly severe radiometric errors, although both classifications differentiated generally the similar areas. Thus, for this study, only through discarding most of the affected bands, which also included valuable information that had to be omitted, satisfying mapping results were possible. To achieve more detailed classification results or material identification, an adequate radiometric correction of the Hyperion data is therefore essential. On the other hand, no further data quality issues were experienced with the ASTER data after the crosstalk correction was applied. Though, an identification of surface types seems to be difficult, the spectral analysis of the ASTER data, plus the possibility to extract elevation data of relative high resolution from the ASTER data was very valuable for the investigations presented here. In conclusion, also regarding the costs and data availability issues beside the quality, the results provided by ASTER data were more valuable for this study compared to the Hyperion data.

REFERENCES

Abrams, M., 2000. The Advanced Thermal Emission and Reflection Radiometer (ASTER): data products for the high spatial resolution imager on NASA's Terra platform. *International Journal of Remote Sensing*, 21(5), pp. 847-859.

Adams, J.B. and Gillespie, A.R., 2006. *Remote Sensing of Landscapes with Spectral Images. A Physical Modeling Approach*. Cambridge, New York.

Bindschadler, R. and Choi, H., 2003. Characterizing and Correcting Hyperion Detectors Using Ice-Sheet Images. *IEEE Transactions on Geoscience and Remote Sensing*, 41(6), pp. 1189-1193.

Broadman, J.W., 1993. *Automated spectral unmixing of AVIRIS data using convex geometry concepts*. Fourth JPL Airborne Geoscience Workshop, JPL Publication, 93-26(1), pp. 11-14.

Bolten, A. and Bubenzer, O., (2006). New elevation data (SRTM/ASTER) for geomorphological and geoarchaeological research in arid regions. *Zeitschrift für Geomorphologie N.F. Suppl.*, 142, pp. 265-279.

Brookes, I.A., 2001. Aeolian erosional lineations in the Libyan Desert, Dakhla Region, Egypt. *Geomorphology*, 39, pp. 189-209.

Brookes, I.A., 1993. Geomorphology and Quaternary geology of the Dakhla Oasis region, Egypt. *Quaternary Science Reviews*, 12, pp. 529-552.

Chang, Ch.-I., 2003. *Hyperspectral Imaging. Techniques for Spectral Detection and Classification*. New York.

CGIAR, 2004. Void-filled seamless SRTM data V1, 2004. International Centre for Tropical Agriculture (CIAT), available from the CGIAR-CSI SRTM 90m Database. http://srtm.csi.cgiar.org (accessed 27 May 2006).

Clark, R.N., 1999. Spectroscopy of Rocks and Minerals, and Principles of Spectroscopy. In: Rencz, A.N. (eds.): *Remote Sensing for the Earth Sciences: Manuel of Remote Sensing. Vol. 3*. New York, pp. 3-58.

Datt, B., McVicar, T.R., Van Niel, T.G., Jupp, D.L.B. & Pearlman, J.S., 2003. Preprocessing EO-1 Hyperion Hyperspectral Data to Support the Application of Agricultural Indexes. *IEEE Transactions on Geoscience and Remote Sensing*, 41(6), pp. 1246-1259.

DigitalGlobe, 2006. *Quickbird Imagery Products. Product Guide.* Revision 4.7.1.

EMA - Egyptian Meteorological Authority, 1996, *Climatic Atlas of Egypt*. Kairo.

Ersdac - Earth Remote Sensing Data Analysis Center, 2003a. *Aster Users Guide*. Part 2 (Ver. 4).

Ersdac - Earth Remote Sensing Data Analysis Center, 2003b. Crosstalk Correction Software User's Guide. http://www.gds.aster.ersdac.or.jp/gds_www2002/service_/ u.tools_e/ cross/GUIDEED.PDF (accessed 06 April 2006).

Folkman, M., Pearlman, J., Liao, L. & Jarecke, P., 2001. EO-1/Hyperion hyperspectral imager design, development, characterization, and calibration. *Hyperspectral Remote Sensing of the Land and Atmosphere, Proceedings of SPIE*, 4151, pp. 40-51.

Fujisada, H., 1995. Design and performance of ASTER instrument. *Proceedings of SPIE*, 2583, pp. 16-25.

Fujisada, H., Bailey, G.B., Kelly, G.G., Hara, S. & Abrams, M.J., 2005. ASTER DEM Performance. *IEEE Transactions on Geoscience and Remote Sensing*, 43(12), pp. 2707-2714.

Fujisada, H., Iwasaki, A. & Seiichi, H., 2001. ASTER stereo system performance. *Proceedings of SPIE, The International Society for Optical Engineering*, 4550, pp. 39-49.

Green, A.A., Berman, M., Switzer, P. & Craig, M.D., 1988. A Transformation for Ordering Multispectral Data in Terms of Image Quality with Implications for Noise Removal. *IEEE Transactions on Geoscience and Remote Sensing*, 26(1), pp. 65-74.

Hirano, A., Welch, R. & Lang, H., 2003. Mapping from ASTER stereo image data: DEM validation and accuracy assessment. *ISPRS Journal of Photogrammetry & Remote Sensing*, 57, pp. 356-370.

Iwasaki, A. & Tonooka, H., 2005. Validation of Crosstalk Correction Algorithm for ASTER/SWIR. *IEEE Transactions on Geoscience and Remote Sensing*, 43(12), pp. 2747-2751.

Iwasaki, A., Fujisada, H., Akao, H., Shindou, O. & Akagi, S., 2002. Enhancement of Spectral Separation Performance for ASTER/SWIR. *Proceedings of SPIE*, 4486, pp. 42-50.

Jenson, J.R., 2005. *Introductory Digital Image Processing. A Remote Sensing Perspective*. Pearson, Prentice Hall, Upper Saddle River.

Kääb, A., Huggel, C., Paul, F., Wessels, R., Raup, B., Kieffer, H., Kargel, J., 2002. Glacier monitoring from ASTER Imagery: Accuracy and Applications. *EARSeL Proceedings*. LIS-SIG Workshop, Bern.

Khurshid, K.S., Staenz, K., Sun, L., Neville, R., White, H.P., Bannari, A., Champagne, C.M. & Hitchcock, R., 2006. Preprocessing of EO-1 Hyperion data. *Canadian Journal of Remote Sensing*, 32(2) pp. 84-97.

Klitzsch, E., List, F.K. & Pöhlmann, G., 1987. Geological map of Egypt 1:500.000, map sheet NG 35 Dakhla. The Egyptian General Petroleum Corporation, CONOCO, Berlin.

Kruse, F.A., Boardman, J.W. & Huntington, J.F., 2003. Comparison of Airborne Hyperspectral Data and EO-1 Hyperion for Mineral Mapping. *IEEE Transactions on Geoscience and Remote Sensing*, 41(6), pp. 1388-1400.

Kruse, F.A., Lefkoff, A.B., Boardman, J.W., Heidebrecht, K.B., Shapiro, A.T., Barloon, P.J. & Goetz, A.F.H., 1993. The Spectral Image Processing System (SIPS). Interactive Visualisation and Analysis of Imaging Spectrometer Data. *Remote Sensing of Environments*, 44. pp. 145-163.

Pearlman, J.S., Barry, P.S., Segal, C.C., Shepanski, J., Beiso, D. & Carman, S.L., 2003. Hyperion, a Space-Based Imaging Spectrometer. *IEEE Transactions on Geoscience and Remote Sensing*, 41(6), pp. 1160-1173.

Research Systems Inc., 2005. *ENVI User's Guide* (ENVI Version 4.2).

Ungar, S.G., Pearlman, J.S., Mendenhall, J.A. & Reuter, D., 2003. Overview of the Earth Observing One (EO-1) Mission. *IEEE Transactions on Geoscience and Remote Sensing*, 41(6), pp. 1149-1159.

Van der Meer, F.D., De Jong, S. M. & Bakker, W., 2003. Imaging Spectrometry: Basic Analytical Techniques. In: Van Der Meer, F. D. & De Jong, S. M. (eds.): *Remote Sensing and Digital Image Processing. Vol. 4. Imaging Spectrometry. Basic Principles and Prospective Applications*. Dordrecht, London.

Waldhoff, G., 2006. *Verbesserung vorhandener geologischer und geomorphologischer Informationen mit Aster-, Hyperion- und Quickbird-Satellitendaten in Ägypten (Dakhla-Oase)*, diploma thesis, unpublished.

Yamaguchi, Y., Kahle, A.B., Tsu, H., Kawakami, T., 1998. Overview of Advanced Spaceborne Thermal Emission and Reflection Radiometer (ASTER). *IEEE Transactions on Geoscience and Remote Sensing*, 36(4) pp. 1062-1071.